

Fractal characteristics of tall tower wind speeds in Missouri

Sarah Balkissoon ^{*}, Neil Fox, Anthony Lupo

Atmospheric Science Program, School of Natural Resources, University of Missouri, USA



ARTICLE INFO

Article history:

Received 2 November 2019

Received in revised form

2 March 2020

Accepted 7 March 2020

Available online 12 March 2020

Keywords:

Hurst exponents

Fractal dimensions

Rescale range analysis

Multifractal detrended fluctuation analysis

Wind speed time series

ABSTRACT

The Hurst exponent H is used to determine the measure of predictability of a time series. The value between 0 and 1 with 0.5 representative of a random or uncorrelated series, $H > 0.5$ and $H < 0.5$ reflect a data set which is persistent and anti-persistent respectively. The fractal dimension can be given from the Hurst exponent. The fractal dimension is a factor of the complexity of which the system is being repeated at various scales. If the fractal dimension does not change with scale it is deemed monofractal if not, multifractal. The Hurst exponents were determined in this study using the Rescale Range Analysis (R/S Analysis) and Multifractal Detrended Fluctuation Analysis (MF-DFA) for monofractal and multifractal investigations respectively. These methods were applied to daily 10 min wind speed time series data for the year 2009 from three locations within Missouri: Columbia, Neosho and Blanchard for three tall tower stations. The results obtained from the monofractal analysis showed minor variations in the Hurst exponents for the three stations and heights for all the months in 2009. These values ranged from 0.7 to 0.9 and its corresponding fractal dimension was ranged between 1.3 and 1.1. The results for the MF-DFA showed that the wind speed time series were multifractal in nature as the Hurst exponents were functions of the scaling parameters. Also, the plots of the Renyi Exponent were non-linear for the stations and the various channels; this is representative of multifractal signals. The fractal dimensions of the time series using multifractal analysis were determined to be greater than these values determined using monofractal analysis. However, there were no indications of consistent increases in the complexity of the systems' multifractality with increasing heights for the various stations' tall towers.

© 2020 Elsevier Ltd. All rights reserved.

1. Introduction

The aim of this study is to determine the internal dynamics of the wind speed time series for three different height levels for three towers in northern, central and southern Missouri. The fractal characteristics of these records provides information on the stochastic processes which generate temporal variations in the series. This information is used in the development of predictive models which ultimately improves the efficacy of wind power as an alternative form of energy.

The subsequent subsections will be an introduction to wind speeds in Missouri, fractals and relationship between the two. Thereafter, the paper gives a description of the data used in this study. Section 3 seeks to explain the monofractal and multifractal methodologies used and section 4 delves into the analysis of the obtained results for each of these procedures. The final section is the conclusion of the major findings.

1.1. Wind speeds in Missouri

Missouri's average wind speed is approximately 4.5 m/s [23] which is above the 3.5 m/s cut-in wind speed required for small turbines to be operational. The wind speed value for Missouri is higher than some states associated with the wind industry which includes Texas, Wyoming, Illinois, California and Colorado [23]. In 2018, six percent of Missouri's electric generation came from renewable energy. Approximately two-thirds of this renewable generation came from wind energy. The wind power generation capacity of 1000 MW was derived from 500 turbines [1]. There is most wind energy potential in the North West regions of Missouri, as seen in Fig. 1 which is an 80 m average annual wind speed map [25].

1.2. Fractals

Fractals are associated with objects that are self-similar, that is, they have the same patterns which occur at different scales and sizes. Mandelbrot [21] stated that is a form of symmetry which is invariant under translations and dilations. These have many details which occur at arbitrary small scales which are too complex to be represented in Euclidean space. Classical geometry and calculus is

* Corresponding author.

E-mail addresses: sarahsharlenebalkissoon@mail.missouri.edu (S. Balkissoon), FoxN@missouri.edu (N. Fox), LupoA@missouri.edu (A. Lupo).

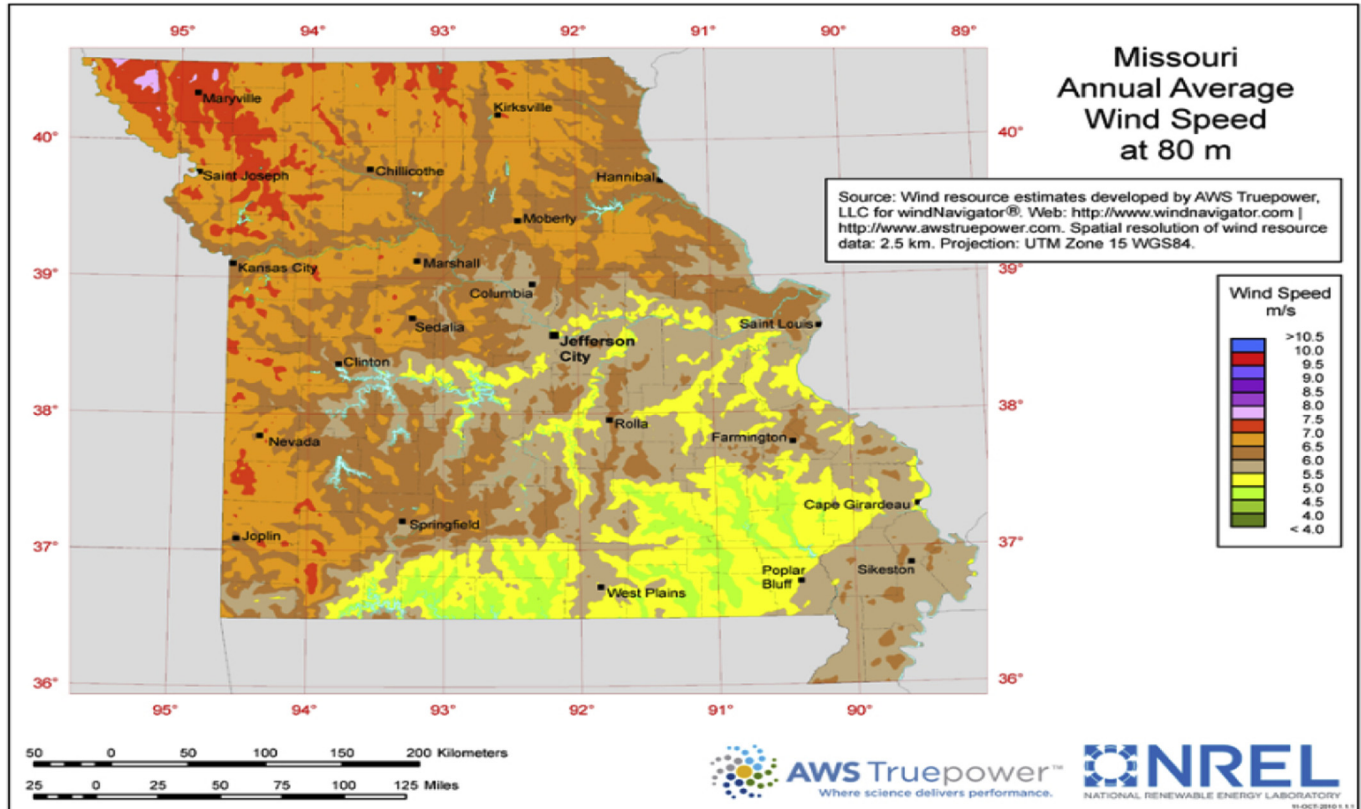


Fig. 1. AWS true power and NREL's wind resource map of Missouri.

not suitable for studying fractals and fractal geometry [8]. According to Mandelbrot, when the fractal or Hausdorff dimension is strictly greater than the topological or Euclidean dimension, the set is considered to be fractal and have fractal geometry [8]; the assigned fractal dimension measures the roughness of the surface [32]. In particular, fractal dimensions can be non-integers which reflects the fact that fractals inhabit space in qualitatively and quantitatively different ways than smooth geometric objects. For example, a smooth curve in the plane is well-approximated by a straight tangent line at each point and hence one dimensional. A fractal, by contrast, does not admit a linear approximation at each point and can have a Hausdorff dimension between one and two. Since the fractal dimension measures the irregularities of a set at various scales, a shape which has a higher fractal dimension is more complex and rough than one that has a lower fractal dimension [3,28].

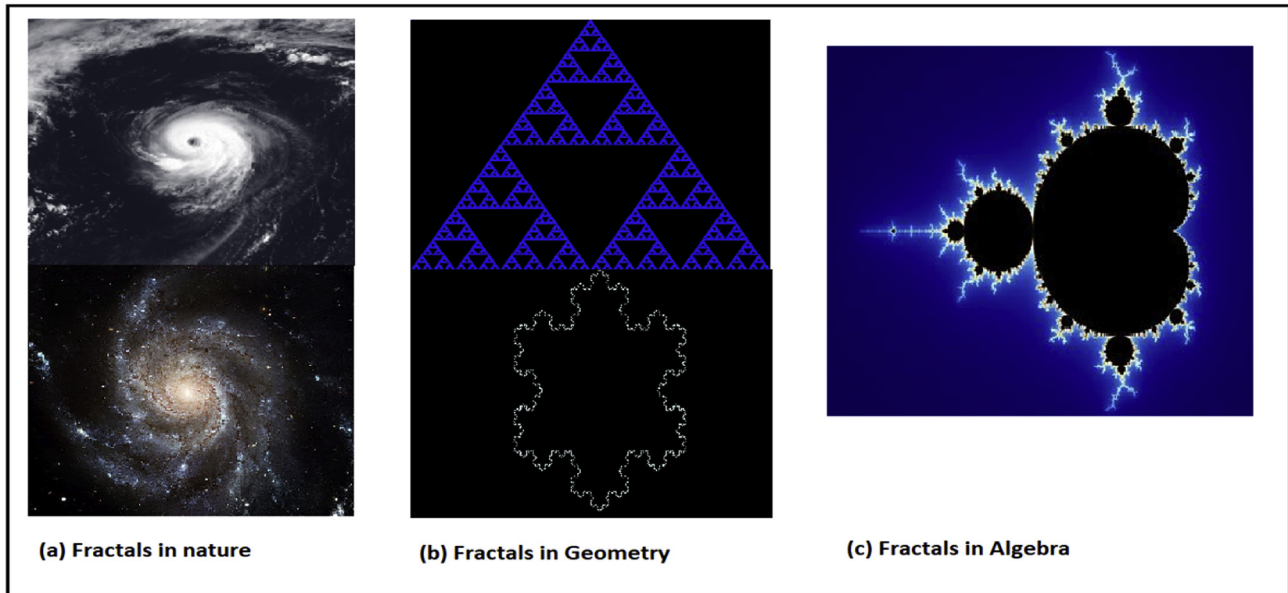
Fractals can be observed in nature, geometry and algebra as well as mathematical physics. In nature fractals can be seen from small scales such as the scale of two to three atomic diameters in metallic glass alloys [24] to large scales of one hundred thousand light years in a spiral galaxy. Coastlines were characterized as fractal in nature by Mandelbrot; the fractal dimension of a Norwegian coastline was determined to be 1.52 and for a British coastline it was given as 1.31 [9,28] whilst the fractal dimension of the space distribution of galaxies less than fifty million light years is 1.23 ± 0.04 [26]. Fractals can also be seen in the nonlinear and chaotic behaviour of river and drainage networks as well as hurricanes which is scale invariant [32].

In geometry, fractals are observed in for example, the triadic Koch Curve and the Sierpinski Triangle; these are intermediate shapes of Euclidean Geometry. The Koch Curve is generated from a less detailed starting shape or initiator in which a similar task is

added on smaller scales thus making the curve more detailed [9,18]. That is, each segment of the generator shape is replaced by a smaller copy of the generator itself. Its fractal dimension is 1.26 which is indicative of its infinite length and its area being 0 [8]. The Sierpinski Triangle is generated by the iterative removal of the middle triangle from the previous reconstruction. The fractal dimension of the Sierpinski Triangle is larger than the Koch Curve, its value is 1.58.

We also see fractals in algebra. They are seen in the beginning of modern Mathematics with the middle third Cantor Sets. These sets display properties of self-similarity and have fine structures in which there are details in arbitrary small scales [18]. This uncountably infinite set is formulated from removing in an iterative manner, the middle third of each interval [8] until the limit of an infinite set of clustered points known as Cantor "dust" is reached [32]. Since from this process, there are 2^n subsets for n iterations having a magnification factor of 3^n , the fractal dimension given by $D = \log(2^n)/\log(3^n)$ is 0.631 [32]. The Mandelbrot Set, which led to the development of complex dynamics, is also fractal. This set is defined as all the complex numbers, c for which the function $f_c(z) = z^2 + c$ stays bounded [19]. The image of the Mandelbrot Set shows all the values of c for which the sequence is bounded and all the values of c outside this set for which $f_c(z)$ goes to infinity. It also shows the rate of which the function tends to infinity as seen in the depiction below, Fig. 2 (c).

There are also fractal connections between non-linear differential equations such as the Navier-Stokes equation [21]. The linear methods of autocorrelation function analysis and spectral analysis are unreliable in the determination of the complex behaviours of non-stationary time series [27]. In fluid motion, turbulence is given as effects of singularities of the Navier–Stokes Equation [21]. To

**Fig. 2.** Fractals.

study this equation, fractal and multifractal models were developed in which the Hausdorff dimension was determined.

1.3. Fractals and wind speed

To evaluate the wind power and wind potential energy, the analysis of the mean wind speeds and frequency distribution need to be done. This is done to mitigate the problems associated with the intermittency of the wind speeds records, in terms of its spatial and temporal variations, when trying to integrate wind power into electrical grids [7]. The internal dynamics of the wind speed time series, that is, its monofractal and multifractal characteristics are used to give information on the stochastic processes which are the generators of these temporal variations. This information is useful in the development of predictive models both theoretical and computational in nature [7]. These wind power forecasting tools increase the efficiency of wind power as an alternative renewable source of energy by reducing the unexpected variations in the wind energy conversions systems (WECS) power generation, thus, reducing operational costs in the electricity generation by reducing the requirements of larger primary reserve capacity [6].

2. Data

In this study, 10 min daily wind speed time series data measured in m/s was used in Missouri, USA for the year of 2009 [12]. Three stations were used in this investigation; Columbia, Blanchard and Neosho. Their location are 038°53.270'N latitude and 092°15.820'W longitude, 040°33.570'N latitude and 095°13.470'W longitude, 036°52.730'N latitude and 094°25.570'W longitude respectively with corresponding site elevations being 255, 328 and 373 m. These are located in North, Central and South Missouri as seen in Fig. 3. The anemometers were placed on various heights and orientations on the towers. For Columbia, Blanchard and Neosho, the anemometer orientations were 120° and 300° for each of the various sites' tall tower heights of 68, 98, 147 m and 61, 97, 137 m and 50, 70, 90 m respectively. Channels 1, 3 and 5 are the wind speed times series of the three consecutive heights at an orientation of 120° and Channels 2, 4 and 6 are wind speed values obtained when anemometers were oriented at 300°. The larger of the wind speed value at each time step for all the

heights were taken for all of the stations. These were labelled Columbia68, Columbia98 and Columbia147, Blanchard61, Blanchard97 and Blanchard137, Neosho50, Neosho70 and Neosho90. These time series for January to December of 2009 were used in the evaluation of the fractal characteristics of wind speeds within Missouri.

3. Methodology

3.1. Monofractal analysis: Rescale Range Analysis (R/S analysis)

There are multiple methods of determining the fractal dimensions of data sets which include the box-counting method, variation method and the Hurst R/S method [3]. The R/S method gives the scale free irregularity and the long term memory or correlation of the series [3]. This method was used by Hurst to compare observed ranges of natural phenomena including river discharges, mud sediments and tree rings [9]. The scale properties of geophysical variables such as precipitation, temperature, sea level and sunspots using R/S analysis were investigated by Lovejoy and Mandelbrot in 1985 and Rangarajan and Sant in 2004 among others [30].

This paper uses the R/S method. To explain the general idea, suppose there is a time series x_i , $i = 1, 2, 3, \dots, N$. The range R_n is defined to be the difference between the maximum and the minimum accumulative departure from the mean of some $n < N$ points. The dimensionless ration $(R/S)_n$ is given by (1).

$$(R/S)_n = \frac{1}{S} \left[\max_n \sum_{i=1}^n (x_i - \langle x \rangle) - \min_n \sum_{i=1}^n (x_i - \langle x \rangle) \right] \quad (1)$$

where

$$\langle x \rangle = \frac{1}{n} \sum_{i=1}^n x_i \quad \text{and} \quad S = \sqrt{\frac{1}{n} \sum_{i=1}^n (x_i - \langle x \rangle)^2} \quad (2)$$

From (1), as $n \rightarrow \infty$, $(R/S)_n \rightarrow Cn^H$ where C is a constant and H is the Hurst Exponent. Thus, from this power law relationship,

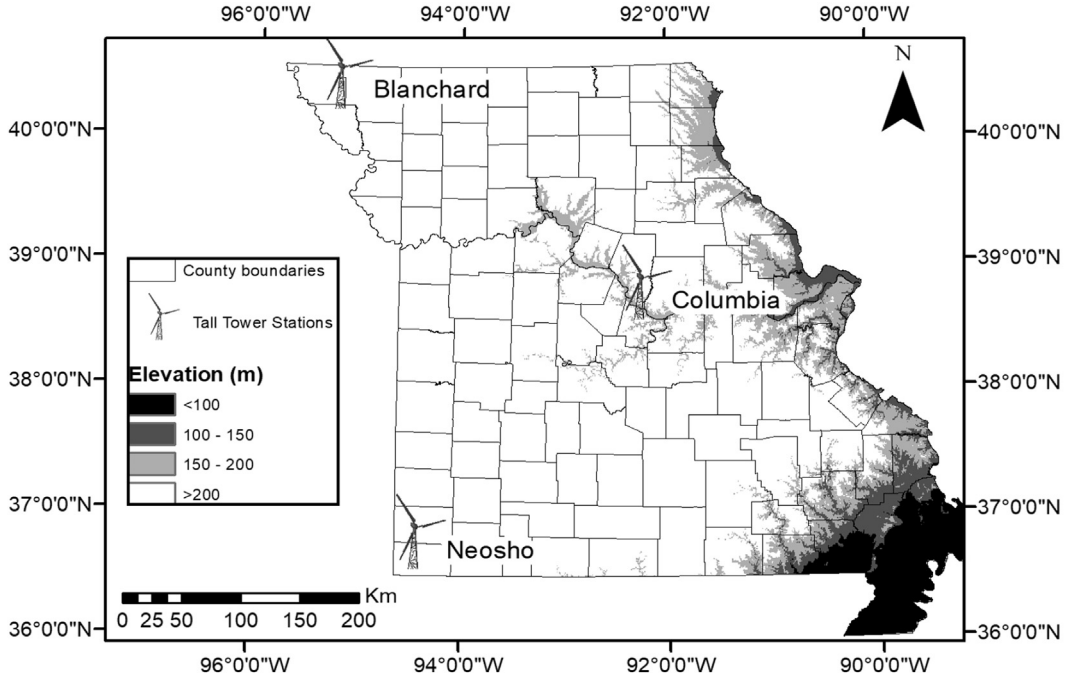


Fig. 3. Study locations within Missouri.

$$\ln(R/S)_n = \ln(C) + H \ln(n). \quad (3)$$

Given (3), a slope of the simple regression line of $\ln(R/S)_n$ against $\ln(n)$ will give the Hurst Exponent H or the degree of correlation. Various values of H corresponds to the following characteristics wind speeds [4].

1. If $H = 0.5$, then wind speed is random or uncorrelated where future data is not determined by current data. This series is called a Brownian time series or a random walk. This series which display no memory is considered to have 'white noise'.
2. If $0.0 < H < 0.5$, then anti-persistence or mean reverting series: the wind speeds have long term negative auto-correlation in adjacent pairs. That is a long term switching between high and lows among adjacent pairs in the series for a long time into the future. A high will be followed by a low and then a high etc. Thus we will have a more rugged or less smooth time series. This occurs because the future values have a tendency to return to the long-term mean. The time series is considered to have 'pink noise' which is related to turbulence.
3. If $0.5 < H < 1.0$, then persistence: the wind speeds have long term positive auto-correlation in adjacent pairs. That is a high value in the series will be followed by another high value for a long time into the future.
4. If $H \approx 1$ or $H = 1$, then there is strong predictability wind speeds or the wind speeds are predictable.

From [20]'s box argument, it is given that the local fractal dimension for self-affine records, D , is $D = 2 - H$.

3.2. Multifractal analysis: Multifractal detrended fluctuation analysis (MF-DFA)

The MF-DFA method was used to study turbulent signals. This procedure was applied to resistor network model, DNA sequences, satellite and microscopic images, financial time series including

stock price fluctuation, traffic time series, quantum dynamical theory, weather records, cloud structure, geology and music among others [13,29,31,33]. The four principle methodologies relating fractal theory to measures are the moment method, the histogram method, the multifractal detrended fluctuation analysis method and wavelet transform modulus maxima method [29]. These analyses are done when the fractal dimension changes with scale and when the time series is non-stationary. There may be multiple scaling exponents which represents different fractal subsets of the series [13]. Unlike the R/S Analysis method, the MF-DFA method can detect non-spurious long-range correlations of a time series when there is non-stationary trends superimposed on it [16,22,33]. The scaling of these intrinsic fluctuation of the time series can be determined despite knowing the origin and the shape of the trends present [22]. This is especially important for this study as the time resolution of the wind speed data sets is 10 min and the analysis is done for a time window of at most one year. Thus the annual trend cannot be estimated and removed from these datasets and as such the trend removing capabilities of MF-DFA is essential [17]. Also, when compared to other multifractal methodologies, the MF-DFA method is less sensitive to the length of the time series and it gives more reliable results using a sample of over 4000 data points [2].

In this paper the MF-DFA is done. To explain the general idea, consider a non-stationary time series of length N , $x(i)$, $i = 1, 2, 3, \dots, N$ with compact support (i.e. $x(i) = 0$ for an insignificant fraction of the series) [13]. The trajectory or profile preserves the variability of the time series whilst simultaneously reducing the noise by removing the non-stationary effects [10]. This profile is given by $Y(i)$, (4) [13].

$$Y(i) = \sum_{k=1}^i [x(k) - \bar{x}] \quad (4)$$

This trajectory is partitioned into N_s non-overlapping intervals of equal length, s , that is, $N_s = [N/s]$. However, N need not be divisible by s thus part of the series may be unaccounted for as the possibility

exist that $[N/s] < (N/s)$. To rectify this, a subdivision is done on the right hand side of the sample. This gives a total of $2N$ partitions or intervals [13]. The local trend is determined by using a polynomial of degree m to fit the trajectories in each of its partitions. The variance is calculated from (5) for the two sets of partitions [13].

monofractal whilst the signal is multifractal if it has non-linear variations with q [7,13,14]. The relationship between this exponent and the Hurst Exponent is $\tau_q = qh_q - 1$. This relationship between the two multifractal scaling exponents was proved in Refs. [13] by considering a stationary positive and normalised

$$F^2(s, v) = \begin{cases} \frac{1}{s} \sum_{i=1}^s [Y[(v-1)s+i] - y_v(i)]^2 & \text{for } v = 1, 2, 3, \dots, N_s \\ \frac{1}{s} \sum_{i=1}^s [Y[(N-(v-N_s)s+i) - y_v(i)]^2 & \text{for } v = N_{s+1}, \dots, 2N_s \end{cases} \quad (5)$$

where $y_v(i)$ is the fitting polynomial for that partition. Finally, the q^{th} order fluctuation, $F_q(s)$, is calculated from the average of all the partitions [13]. Please see (6).

$$F_q(s) = \left[\frac{1}{2N_s} \sum_{v=1}^{2N_s} \left[F^2(s, v) \right]^{\frac{1}{q}} \right]^q \quad (6)$$

where $q \neq 0$ and $s \geq m + 2$, m is the degree of the fitting polynomial. The scale was chosen to be 10: 100 and m was chosen as 1. Thus the inequality for which $F_q(s)$ was defined, holds.

The multifractality of the time series is caused by different long term correlations in the sample. MF-DFA can be used to determine multiple scaling exponents and spectrum parameters to classify the complexity and dynamics of the time series unlike monofractal analysis which characterizes the scaling property by one exponent for the entire data set. The four multi-fractal analyses done in this paper are as follows:

1. $\log(F_q(s))$ against $\log(s)$ where s is the scale and F_q is the q^{th} order fluctuation average. If q is negative then small fluctuations are enhanced and if q is positive then it enhances large fluctuations. To determine if long term correlation exist in the signal there should be a power law variation where F_q increases as a power of s . Thus, the generalized Hurst Exponent is the slope of this log-log plot as $F_q \approx s^{h_q}$ [11,13,14] and there is a linear relation in log plot for the various q values.
2. h_q against q or the dependence of the general Hurst Exponent on q . For monofractal time series h_q is independent of q [11]. The local trend of each segment is calculated from the least square fit of the series and the variance of each segment. Since the scaling does not change, the trend over each segment is the same. For multifractal time series h_q is dependent on q . This dependence of h on q is caused by the fluctuations of scales both large and small. For large positive q values, there will be larger deviations from the least square fit thus larger variances $F^2(s, v)$ [11]. These large variances are also reflected in the q^{th} order fluctuation and as such there is a relation between the large fluctuations and the Hurst Exponent, h_q . Large fluctuations for multifractal time series implies smaller h_q values [13]. Similarly, for negative values of q , there are smaller variances and small fluctuations are characterized by larger scaling exponents h_q [13]. Thus we have for a monofractal data set there will be one exponent for all scales whereas for a multifractal time series, h_q monotonically decreases with increasing q .
3. τ_q against q or the q^{th} order mass exponent. τ_q is called Rényi Exponent. If τ_q varies linearly with q , then the time series is

sequence, substituting its simplified version of the variance, standard fluctuation analysis into (6) and comparing it with the box probability for the standard multifractal formalism for the normalised series.

4. $f(\alpha)$ against α or the multifractal spectrum. If the signal is a single scale fractal series then $f(\alpha)$ is a constant. A bell-like shape is given if the signal displays multifractal tendencies [11]. This function is related to Rényi Exponent by the relation $f(\alpha) = q\alpha - \tau_q$ where α is Hölder Exponent and $\alpha = \frac{d\tau_q}{dq}$ [13]. Since, $\tau_q = qh_q - 1$, $\alpha = h_q + q\frac{dh}{dq}$ and $f(\alpha) = q[\alpha - h_q] + 1$. Some multifractal spectrum parameters include position of max α_0 , width of spectrum W and skew parameter r . The width of the spectrum is given by $W = \alpha_{max} - \alpha_{min}$ and the skew parameter is $r = \frac{\alpha_{max} - \alpha_0}{\alpha_0 - \alpha_{min}}$ [7]. The width of the spectrum determines the degree of the multifractality of the signal where a larger spectrum width coincides with greater dynamics of the data set and stronger multifractality [7,15]. The skewness parameter is classified as $r = 0$ for symmetry, $r > 1$ for a right skewed spectrum and $r < 1$ for a left skewed spectrum. The dominant fractal exponent describing the scaling of small or large fluctuations is also determined by r . For a right skew spectrum, the fractal exponent describes the scaling of small fluctuations whilst large fluctuations are described by a left skew spectrum [7]. The more complex and multifractal signals are signals where α_0 and W are large values as well as $r > 1$ or is right skewed [7].

4. Analysis of results

4.1. Raw data

The monthly mean wind speeds for the various channels in Columbia, Blanchard and Neosho were plotted in Fig. 4. Average max wind speeds were recorded and determined for January to December of 2009 in Columbia and for January to August and January to October in Blanchard and Neosho respectively. From the plot, we see a similarity in terms of the wind speed patterns for all three stations. We see that the months of January to April and October to December are peak months whilst there is a decrease in average wind speeds during the period of May to September. From the average wind speeds in Columbia and Neosho, it is evident that the maximum to minimum wind speeds for each month coincided with the highest to lowest height levels, Columbia147 to Columbia68 and Neosho90 to Neosho50. For Blanchard, this holds true with the exception of intermediate height time series, Blanchard97, which had the lowest monthly averages of all the stations.

It was observed that the maximum wind speeds of all the stations for all the months came from the greatest tall tower heights of Blanchard137 and Columbia147. Also, with the exception of

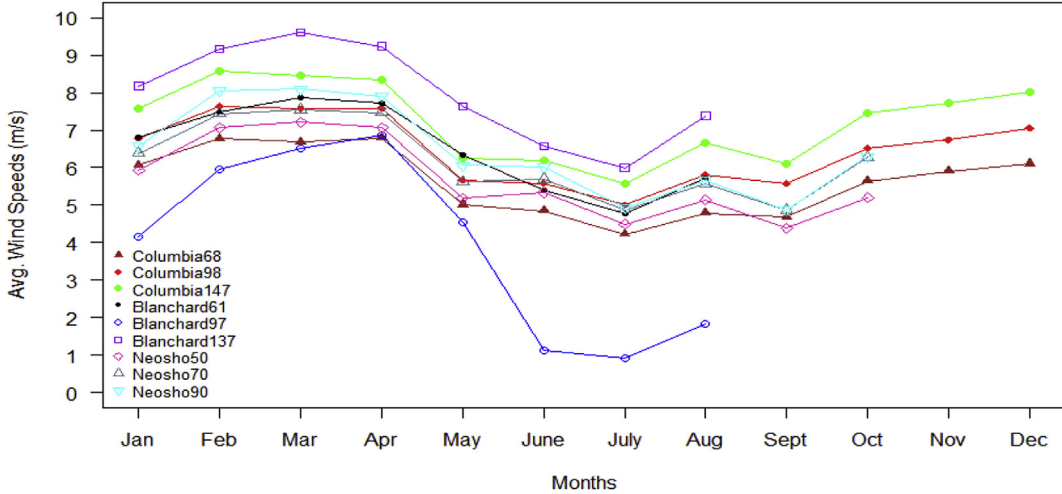


Fig. 4. Average max wind speeds in columbia, blanchard and neosho in 2009.

Blanchard97, the lowest average wind speeds came from the Columbia and Neosho stations at the lowest heights of 68 m and 50 m respectively.

4.2. Monofractal analysis

Figs. 5(a)–(c) show the monofractal Hurst Exponents for Columbia, Blanchard and Neosho respectively in 2009. From the results obtained there is no clear distinction in the Hurst Exponent values from the various series for all the stations thus indicating that the fractal dimensions of the wind speeds did not alter significantly with increasing heights. The fractal dimensions were consistently in the range of 1.1–1.3 for all the stations and months. This may have been as a result of similar variations of wind speeds with height. As such we expect the Hurst exponents and the fractal dimensions to be similar.

In Fig. 5(c), it is observed that Neosho had the least monthly variations in the fractal dimensions for all of the heights when compared to the other two stations; its fractal dimensionality was determined to be 1.2 (to one decimal place). However of all the tall towers, this station gives the wind speeds taken over the smallest range of heights. It was determined that the numerically small variations in fractal dimensions of the other two stations, given by Figs. 5(a) and (b) were not similarly changing with height and months when compared to Fig. 4. For Columbia, the greatest fractal dimensions occurred in February and December at the lowest height of 68 m and in August at heights of 98 m and 147 m whilst the least fractal dimensions occurred in January for all height levels. Similarly, for Blanchard the fractal dimension of approximately 1.3 was observed for all heights in February. This was also noted in July and August with the exception of Blanchard61 and Blanchard97 respectively.

The Hurst Exponents were determined to be in the range of 0.7–0.9. R/S Analysis was used to show that the wind speeds investigated in this study does not follow a random Gaussian process but rather a long term autocorrelation. Since $0.5 < H < 1.0$, this implies that the wind speed had a long term positive autocorrelation in adjacent pairs where a high value will be followed by another high value for a long time into the future. That is, its fluctuations are interconnected because there exist a statistical order in the dynamics of the system [30]. There will be less peaks than a random series and it will be less rugged than an anti-persistent system [4]. This is consistent with a study done by Fortuna and

Guariso [11] in which daily and monthly wind speed time series were analyzed from regions within the USA and Italy using two methods, Box Counting Method, D and the Hurst Exponent R/S Range Analysis Method, H . The wind speeds for these regions were determined to be fractal also because the average D values were 1.19 and 1.41 for daily and hourly mean wind speeds respectively. More complexity was discovered for hourly wind speeds than the daily wind speeds as indicated from its higher fractal dimensions. This is indicative of greater details and finer structures which the greater temporal resolution provides. This numerical value is in agreement with our study even though different locations and time scales were used.

4.3. Multifractal analysis

As in Figs. 6(a)–(c), Scaling function order F_q , it is evident that for all of the heights, there were increases in F_q as q values were increased from -5 to 0 to 5 for all of the three tall tower stations. We see that $\ln(F_q)$ varies linearly with $\ln(s)$ for a scale of 10–100 days with the generalized Hurst Exponent being the slope; this indicates a scale dependence which is characteristic of multifractality. Also, it is observed that as s increases, the distances among the different q values decreases. This occurs because for small segments (small s values), localized periods of small fluctuations given by negative q values, can be differentiated from periods of large fluctuations given by positive q values. This is unlike large segments (large s values) which includes both small and large fluctuations where the tendency for the magnitude differences to cancel occur [27]. The hypothesis of the multifractal nature of wind speeds were also supported by the study of Fortuna and Guariso [11] for daily mean wind speeds recorded at Aberdeen from 2000 to 2012 in which the regression lines varied for differing q orders. Thus, the Hurst Exponents given by the slope of the plots were changing also for these sets. Similar results were also observed in another study in Northeastern Brazil, Petrolina for both hourly wind speed and max wind speed [7]. Thus we see that for temporal variations of data ranging from the 10 min to daily time series, all showed multi-fractal characteristics.

As seen in Figs. 7(a)–(c), dependence of the Generalize Hurst Exponent, it is seen that q increases as h_q decreases monotonically for all height levels. This is also noted in the slopes of Figs. 6(a)–(c). Larger fluctuations corresponded with smaller h_q values and similarly, smaller fluctuations corresponded with larger scaling

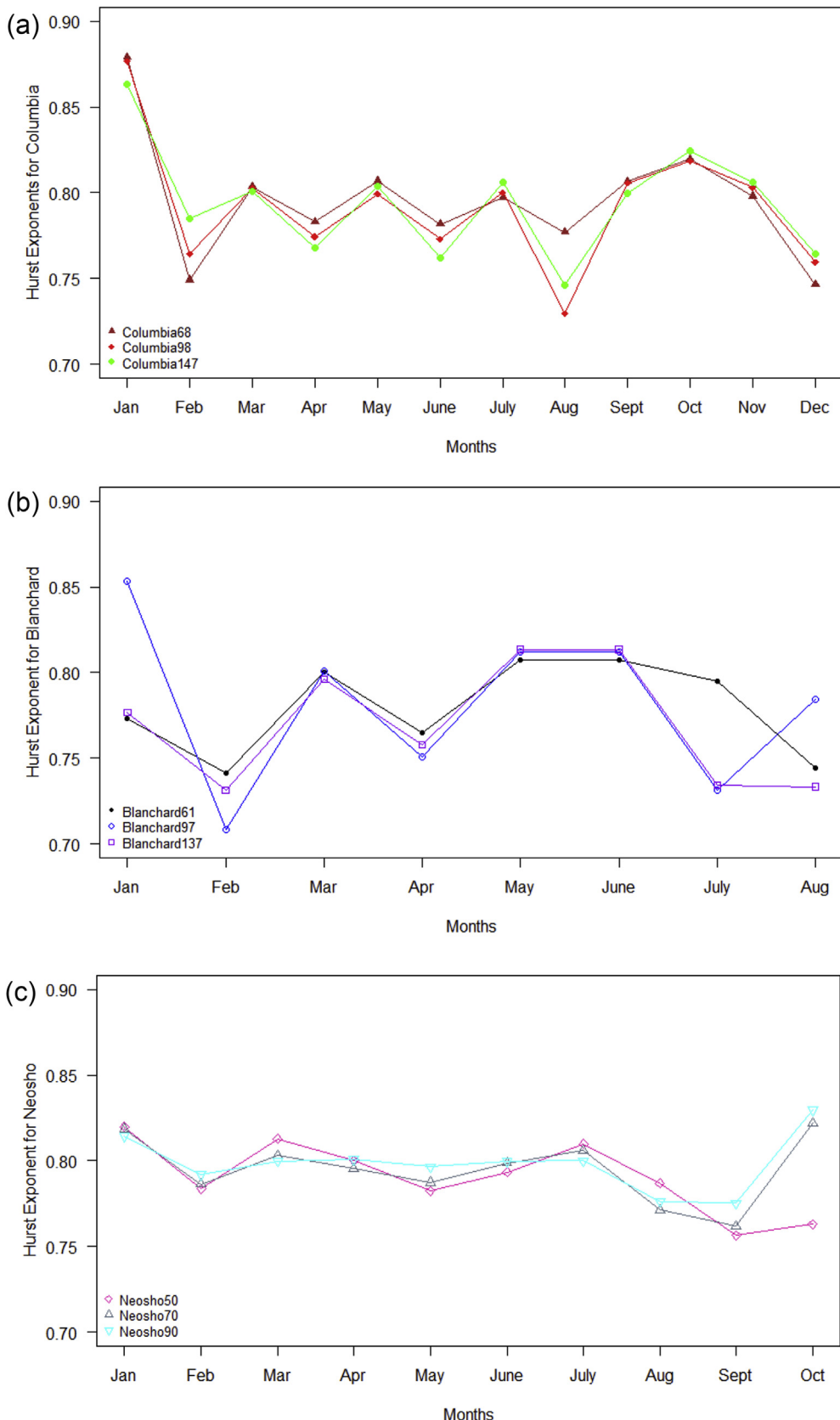


Fig. 5. (a) Hurst Exponents for Columbia in 2009 (dark red - Columbia68, red-Columbia98, green- Columbia147). (b) Hurst Exponents for Blanchard in 2009 (black- Blanchard61, blue- Blanchard97, purple- Blanchard137). (c) Hurst Exponents for Neosho in 2009 (pink-Neosho50, grey- Neosho70, cyan-Neosho90). (For interpretation of the references to colour in this figure legend, the reader is referred to the Web version of this article.)

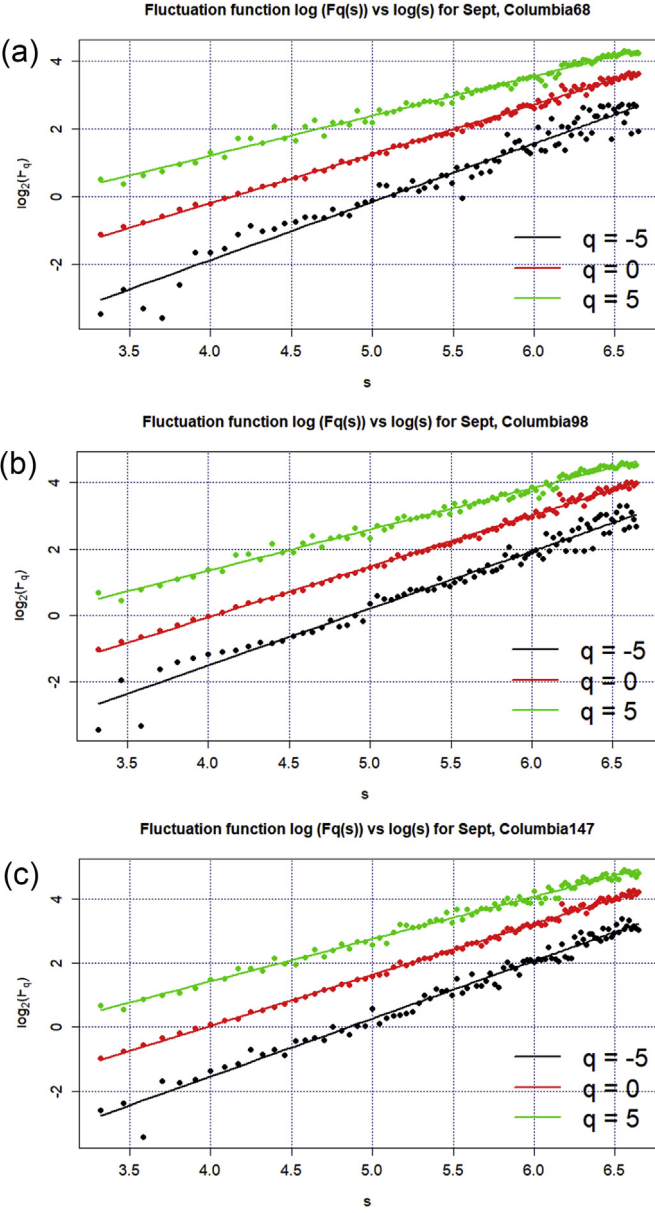


Fig. 6. (a) MF-DFA performed on 10 min wind speed data in Columbia for tower height 68 m - Scaling function order F_q . Plot of $\log(F_q)$ against $\log(s)$. (b) MF-DFA performed on 10 min wind speed data in Columbia for tower height 98 m - Scaling function order F_q . Plot of $\log(F_q)$ against $\log(s)$. (c) MF-DFA performed on 10 min wind speed data in Columbia for tower height 147 m - Scaling function order F_q . Plot of $\log(F_q)$ against $\log(s)$.

exponents. It is observed that for Columbia68, Columbia98 and Columbia147 in the month of September, when q varied from -5 to 5 , h_q decreased from 1.7196 to 1.1730 , 1.7171 to 1.2429 and 1.8055 to 1.3216 respectively. Since there is a range of values for the various scales for all height levels then these are indicative of multifractal series. This is also in agreement with a study done by Kavasseri and Nagarajan [14] for four sites with significant wind potentials in North Dakota where hourly data was taken from a cup anemometer at a height of 20 m. They determined that for one of the sites, when q increased from -6 to 6 , the slope decreased from 0.88 to 0.6989 .

The Generalized Hurst h_q is related to the Hurst Exponent, H , by $h(2) = H$ for stationary time series where $0 < h(q = 2) < 1$ [22]. For non-stationary time series, the scaling exponent of $F_q(s)$ is characterized by $h(q = 2) > 1$ and the relationship between H and h_q is

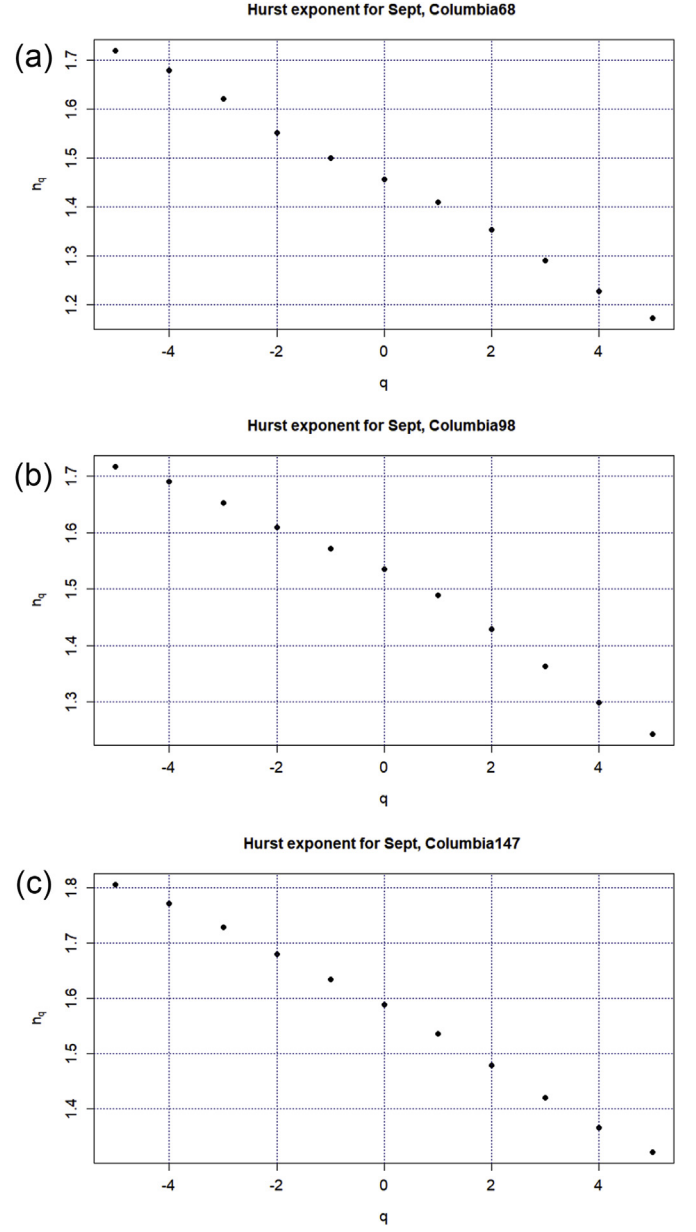


Fig. 7. (a) MF-DFA performed on 10 min wind speed data in Columbia for tower height 68 m - Dependence of Gen Hurst Exp on q . Plot of h_q against q . (b) MF-DFA performed on 10 min wind speed data in Columbia for tower height 98 m - Dependence of Gen Hurst Exp on q . Plot of h_q against q . (c) MF-DFA performed on 10 min wind speed data in Columbia for tower height 147 m - Dependence of Gen Hurst Exp on q . Plot of h_q against q .

given by $H = h(q = 2) - 1$. This is proved in Ref. [22]. For September, $h(2)$ values for Columbia68, Columbia98 and Columbia147 were determined to be 1.3536 , 1.4290 and 1.4779 respectively. This indicates a non-stationary process with long range correlation behaviour [31]. The corresponding Hurst exponents as well as fractal dimensions, D , for this month and stations at the three heights are 0.3536 , 0.4290 , 0.4779 and 1.6464 , 1.571 , 1.5221 . These results gives higher fractal dimensions than the monofractal analysis for the time series data. It also showed that the wind speed time series are displaying long-term anti-persistence correlations as in a study done by Refs. [34] in which the multifractality of multivariate wind speed for both indoor and outdoor records were examined.

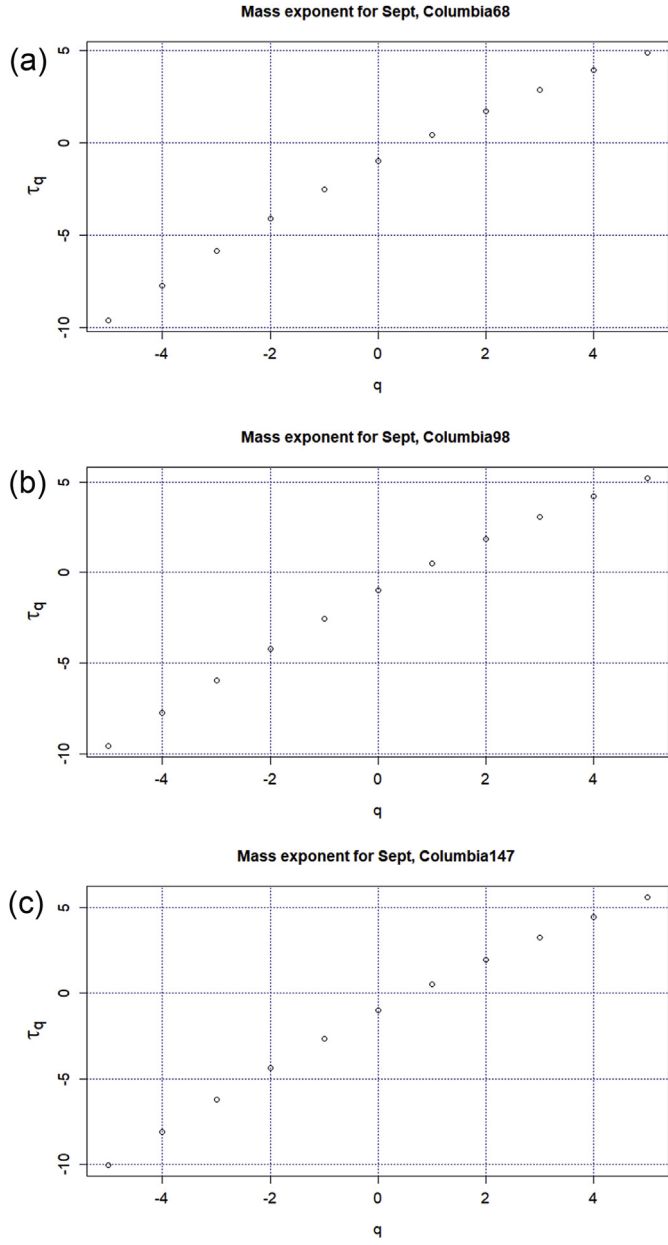


Fig. 8. (a) MF-DFA performed on 10 min scaled wind speeds in Columbia for tower height 68 m - q-order Mass exponent. Plot of τ_q against q . (b) MF-DFA performed on 10 min scaled wind speeds in Columbia for tower height 98 m - q-order Mass exponent. Plot of τ_q against q . (c) MF-DFA performed on 10 min scaled wind speeds in Columbia for tower height 147 m - q-order Mass exponent. Plot of τ_q against q .

From Figs. 8(a)–(c), it is noted that Rényi Exponents τ_q have non-linear variations with q . This is also characteristic of the wind speeds taken at the three heights of each tall tower, being multifractal signals. This is also noted from the hourly non-stationary time series MF-DFA by de Figueirido et al. [7] between the years 2008 and 2011.

The last of the analyses is the multifractal spectrum, Figs. 9(a)–(c). The spectra of $f(\alpha)$ against α are not constant thus indicating that the series are not single scale fractal signals for all the months and height levels in Columbia, Blanchard and Neosho. The results obtained, the signals displayed multifractal tendencies by producing spectra of single-hump like features or bell-shapes with the exception of June C147, July C147, Aug C98 and Dec C68,

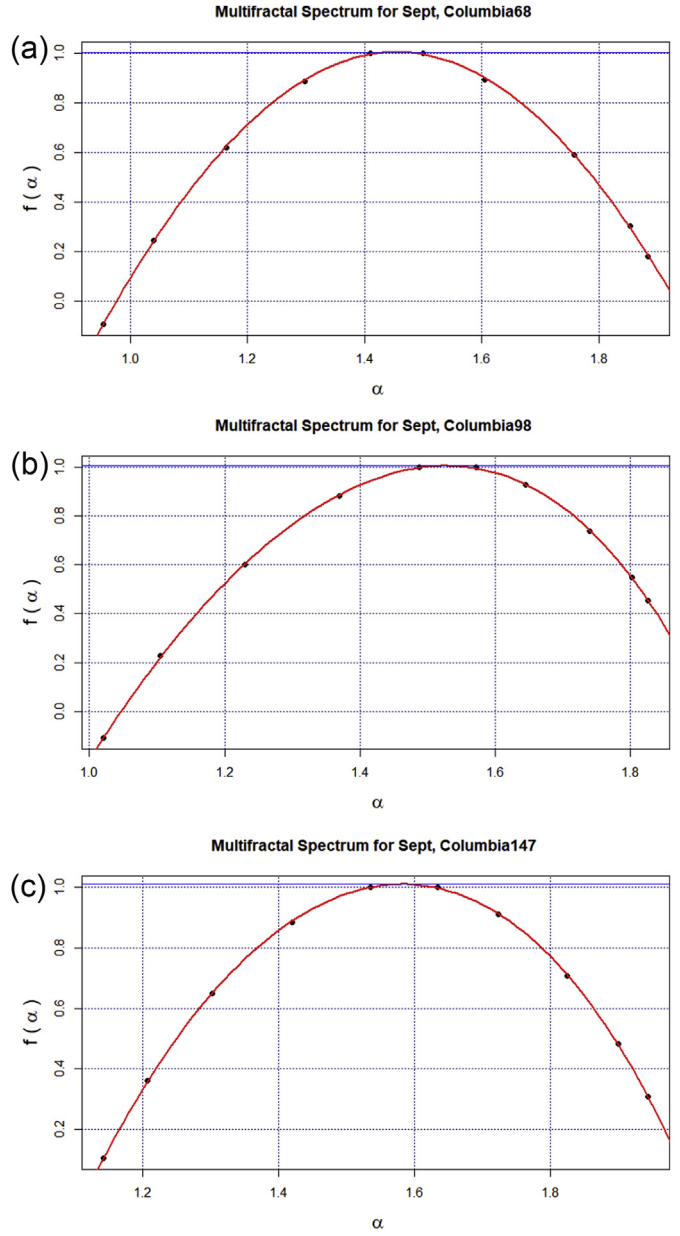


Fig. 9. (a) MF-DFA performed on 10 min scaled wind speeds in Columbia for tower height 68 m - Multifractal Spectrum. Plot of $f(\alpha)$ against α . (b) MF-DFA performed on 10 min scaled wind speeds in Columbia for tower height 98 m - Multifractal Spectrum. Plot of $f(\alpha)$ against α . (c) MF-DFA performed on 10 min scaled wind speeds in Columbia for tower height 147 m - Multifractal Spectrum. Plot of $f(\alpha)$ against α .

C98, C147, Jan B97 and B137, Feb B97, Mar B97, Apr B61 and B97, July B137, Jan N50, N70 and N90, Mar N90, Sept N70 and N90, Oct N90. This may have been as a result of artifacts being contained in the observational data which makes the determination of the long-term correlations and multifractality of the records difficult. These artifacts may include additive random noise and short term correlations. Additive random noise can be derived from the limitations in the accuracy of the measuring instruments and short term correlations can be given from the short time scale of our study. The latter induces a strong persistence which is superimposed on the long-range correlations [17]. These artifacts have been proven in Ref. [17] to cause various degrees of underestimation of h_q for small and negative moments which are most affected by noise. Ludescher et al. [17] also proved that the multifractality of the positive

Table 1

The Multifractal Spectrum Parameters for Columbia, Blanchard and Neosho for the three height levels and months in 2009.

| Description | | Columbia, C | | | | Blanchard, B | | | | Neosho, N | |
|-------------|---------------|-------------|----------------|----------------|-------|--------------|-------|-------|------|-----------|--|
| Month | Heights | α_0 | α_{max} | α_{min} | w | r | w | r | w | r | |
| Jan | C68 B61 N50 | 0.83 | 1.46 | 0.57 | 0.89 | 2.42 | 0.70 | 1.06 | 1.29 | 4.49 | |
| Jan | C98 B97 N70 | 0.85 | 1.48 | 0.53 | 0.95 | 1.97 | 1.37 | 0.18 | 1.31 | 4.54 | |
| Jan | C147 B137 N90 | 0.80 | 1.48 | 0.43 | 1.05 | 1.84 | 1.61 | 0.31 | 1.26 | 4.07 | |
| Feb | C68 B61 N50 | 1.36 | 1.57 | 0.93 | 0.64 | 0.49 | 0.61 | 0.56 | 0.57 | 0.43 | |
| Feb | C98 B97 N70 | 1.39 | 1.63 | 1.00 | 0.63 | 0.62 | 11.86 | 13.83 | 0.60 | 0.50 | |
| Feb | C147 B137 N90 | 1.40 | 1.58 | 1.06 | 0.52 | 0.53 | 0.64 | 0.45 | 0.74 | 0.72 | |
| Mar | C68 B61 N50 | 1.29 | 1.47 | 0.93 | 0.54 | 0.50 | 0.53 | 0.43 | 0.03 | 0.98 | |
| Mar | C98 B97 N70 | 1.31 | 1.48 | 0.92 | 0.56 | 0.44 | 14.78 | 0.05 | 0.56 | 0.40 | |
| Mar | C147 B137 N90 | 1.40 | 1.63 | 0.93 | 0.70 | 0.49 | 1.89 | 0.80 | 0.62 | 0.59 | |
| Apr | C68 B61 N50 | 1.37 | 1.57 | 1.17 | 0.4 | 1.00 | 2.85 | 3.45 | 0.7 | 0.75 | |
| Apr | C98 B97 N70 | 1.38 | 1.55 | 1.22 | 0.33 | 1.06 | 10.93 | 0.07 | 0.73 | 1.03 | |
| Apr | C147 B137 N90 | 1.43 | 1.61 | 1.22 | 0.39 | 0.86 | 0.62 | 0.72 | 0.81 | 1.31 | |
| May | C68 B61 N50 | 1.29 | 1.44 | 0.94 | 0.50 | 0.43 | 0.62 | 0.72 | 0.81 | 0.72 | |
| May | C98 B97 N70 | 1.38 | 1.80 | 0.95 | 0.85 | 0.98 | 0.72 | 0.60 | 0.99 | 0.90 | |
| May | C147 B137 N90 | 1.45 | 1.82 | 1.01 | 0.81 | 0.84 | 0.73 | 0.62 | 0.85 | 0.55 | |
| June | C68 B61 N50 | 1.29 | 1.68 | 0.76 | 0.92 | 0.74 | 1.04 | 0.65 | 0.96 | 0.68 | |
| June | C98 B97 N70 | 1.35 | 1.69 | 0.83 | 0.86 | 0.65 | 1.04 | 0.65 | 0.99 | 0.77 | |
| June | C147 B137 N90 | 7.79 | 8.69 | 0.86 | 7.83 | 0.13 | 1.09 | 0.68 | 2.09 | 1.38 | |
| July | C68 B61 N50 | 1.34 | 1.68 | 1.06 | 0.62 | 1.21 | 0.85 | 0.77 | 0.8 | 0.74 | |
| July | C98 B97 N70 | 1.40 | 1.75 | 1.10 | 0.65 | 1.17 | 0.85 | 0.77 | 0.66 | 0.61 | |
| July | C147 B137 N90 | 1.57 | 2.96 | 1.11 | 1.85 | 3.02 | 1.73 | 0.35 | 0.65 | 0.59 | |
| Aug | C68 B61 N50 | 1.30 | 1.46 | 0.97 | 0.49 | 0.48 | 0.75 | 0.56 | 0.81 | 0.56 | |
| Aug | C98 B97 N70 | 1.62 | 2.89 | 1.03 | 1.86 | 2.15 | 0.75 | 0.56 | 0.74 | 0.45 | |
| Aug | C147 B137 N90 | 1.54 | 1.89 | 1.09 | 0.8 | 0.78 | 0.76 | 0.46 | 0.8 | 0.74 | |
| Sept | C68 B61 N50 | 1.45 | 1.94 | 0.97 | 0.97 | 1.02 | | | 8.46 | 0.11 | |
| Sept | C98 B97 N70 | 1.53 | 1.92 | 1.04 | 0.88 | 0.80 | | | 7.34 | 0.12 | |
| Sept | C147 B137 N90 | 1.58 | 2.01 | 1.11 | 0.9 | 0.91 | | | 0.89 | 1.07 | |
| Oct | C68 B61 N50 | 1.29 | 1.70 | 0.92 | 0.78 | 1.11 | | | 6.08 | 0.13 | |
| Oct | C98 B97 N70 | 1.32 | 1.53 | 0.94 | 0.59 | 0.55 | | | 0.70 | 0.94 | |
| Oct | C147 B137 N90 | 1.34 | 1.52 | 0.91 | 0.61 | 0.42 | | | 0.69 | 0.77 | |
| Nov | C68 B61 N50 | 1.37 | 1.78 | 1.05 | 0.73 | 1.28 | | | | | |
| Nov | C98 B97 N70 | 1.43 | 1.88 | 1.07 | 0.81 | 1.25 | | | | | |
| Nov | C147 B137 N90 | 1.46 | 1.58 | 1.18 | 0.92 | 1.81 | | | | | |
| Dec | C68 B61 N50 | 2.70 | 12.19 | 0.94 | 11.25 | 5.39 | | | | | |
| Dec | C98 B97 N70 | 1.75 | 4.06 | 1.06 | 3.00 | 3.35 | | | | | |
| Dec | C147 B137 N90 | 2.92 | 13.45 | 1.05 | 12.4 | 5.63 | | | | | |

moments may be corrupted. These graphical anomalies of h_q were noted in our results corresponding with the spectra which did not depict a bell-like shape. This is due to the fact that $f(\alpha)$ is obtained from Legendre transform which utilizes information on the moments [17].

The MF-DFA parameters of W and r were determined from the singularity spectrum as given by Table 1. The width of the spectrum is a measure of multifractality of the time series where a large width characterizes a finer signal structure which is more multifractal in nature. A width which tends to zero, however, is representative of a series that has one scaling exponent or one that is monofractal. From the results of this study, there was no indication of a consistent trend showing that the multifractality increases with increasing height from C69 to C147, B61 to B137 and N50 to N90. From the asymmetry parameter, r , for C68 to C147, some of the spectra are left skewed whilst others are right, also indicating that there is no trend of a dominant fractal exponent as the heights are increased. For Blanchard, predominantly, the dominant scaling is of large fluctuations as described by left skew parameter r . This is indicative of a the prevalence of a fractal exponent describing a structure that is less fine.

It was seen in Kavasseri and Nagarajan [14] that the spectrum widths for their data taken at height of 20 m were 0.4475–0.4862. In de Figueirôdo et al. [7] the spectrum widths were 0.24 and 0.51 for average and maximum wind speed data taken from a meteorological station of altitude 370.46 m. From this study, the spectral widths for Columbia's single humped multifractal spectra, at tower heights of 68, 98 and 147 m and site elevation of 255 m were given by $0.33 \leq W \leq 1.05$. This range is similar to the spectral width

parameter values obtained by Laib et al. [15] for 119 stations in Switzerland using 10 min time series data; W was ranged between 0.206 and 1.15. For Blanchard and Neosho, the single hump widths ranged between 0.53 to 1.09 and 0.56 to 0.99 with the exception of Mar B137 and June N50 whose width values was 1.89 and 2.09 respectively. These differences in the widths from the three stations do not show as much variations as the study done by Ref. [10] in China using daily wind speed data. However, they represent the non-universal multifractal characteristic of wind speeds due to varying space and time dynamics. The parameters changes with location and heights levels and is as a result of different atmospheric circulation patterns. This is especially valid for wind speeds as seen from a climatic study of 31 years done by Ref. [2], using meteorological variables of precipitation, global radiation, wind speed, relative air humidity and air temperature, the greatest differences in the widths of the spectra were observed for wind speeds between Polish sites. The irregular fluctuations and complexity of the wind speeds is dependent on numerous factors which includes temperature, pressure gradient, turbulence and topography of the various sites [34].

5. Conclusion

It was determined that winds speeds within Missouri, using monofractal analysis, were determined to be persistent as the Hurst exponent was greater than 0.5 for the three stations at the various height levels for all the months in 2009 using 10 min data. There were no consistent increases in the fractal dimensions as the height levels were increased nor were they changes in the fractal

dimension with months which corresponded with the average max wind speeds for the three stations.

From the MF-DFA, the wind speeds in Columbia, Blanchard and Neosho were determined to be multifractal in nature as there were changes in the fractal dimensions with scales. The fractal dimensions of the time series using multifractal analysis were determined to be greater than these values determined using monofractal analysis. However, the multifractality of the data sets, determined from the widths of the inverse parabolic shaped spectra, did not show any consistently increasing trend with heights which would have been indicative of greater complexity and finer structures of the wind speed records. The range of the widths which changed from various tower locations, reflects the non-universal multifractal characteristics of wind speeds and the different atmospheric circulation patterns. From the asymmetry parameter they were no evidence of a dominating fractal exponent as the heights were increased.

Future work entails forecasting using Empirical Dynamical Modelling (EDM), having already established in this paper that the natural system of wind speeds from tall towers within Missouri are complex, dynamical and chaotic. In EDM, the wind time series will be used to construct the attractor from a mathematical theory developed by Takens. The dynamics of the system can be determined by a single time series as shown from Takens' embedding theorem. From the embedding theorem, each variable contains information about the other variables and thus, the wind speed time series and its time lagged co-ordinates will be utilized to study the system [5].

Declaration of competing interest

The authors declare that they have no known competing financial interests or personal relationships that could have appeared to influence the work reported in this paper.

CRediT authorship contribution statement

Sarah Balkissoon: Conceptualization, Methodology, Software, Validation, Formal analysis, Writing - original draft, Writing - review & editing. **Neil Fox:** Conceptualization, Methodology, Formal analysis, Resources, Writing - review & editing, Supervision, Project administration. **Anthony Lupo:** Conceptualization, Methodology, Formal analysis, Writing - review & editing, Supervision, Project administration.

Acknowledgement

The study was made possible through the Fulbright Foreign Student Program. The authors will like to thank Dr. Sue Ellen Haupt from NCAR, Dr. Samuel Walsh and Dr. Charles Li from University of Missouri, Department of Mathematics for their help and suggestions throughout this research project. The authors will like to extend their gratitude to Dr. Bahtiyar Efe and Ms. Katherine Rojas for their invaluable contributions in development of this project. We also extend our gratitude to the anonymous reviewers for all of their suggestions. This work was supported in part by the Missouri Experimental Project to Stimulate Competitive Research (EPSCoR) of National Science Foundation, under Award Number IIA-1355406. Any opinions, findings, and conclusions or recommendations expressed in this material are those of the authors and do not necessarily reflect the views of the National Science Foundation. Funding for data collection was provided by Missouri Department of Natural Resources, Ameren UE, Aquila, Columbia Water and Light, Kansas City Power and Light, and Empire District Electric Company.

References

- [1] U. E. I. Administration, Missouri State Profile and Energy Estimates, 2019.
- [2] P. Baranowski, J. Krzyszczak, C. Slawinski, H. Hoffmann, J. Kozyla, A. Nierobca, K. Siwek, A. Gluza, Multifractal analysis of meteorological time series to assess climate impacts, *Clim. Res.* 65 (2015) 39–52.
- [3] M. Breslin, J. Belward, Fractal dimensions for rainfall time series, *Math. Comput. Simul.* 48 (4–6) (1999) 437–446.
- [4] E. Cadena, R. Campos-Amezcu, W. Rivera, M.A. Espinosa-Medina, A.R. Méndez-Gordillo, E. Rangel, J. Tena, Wind speed variability study based on the hurst coefficient and fractal dimensional analysis, *Energy Science & Engineering* 7 (2) (2019) 361–378.
- [5] C.-W. Chang, M. Ushio, C.-h. Hsieh, Empirical dynamic modeling for beginners, *Ecol. Res.* 32 (6) (2017) 785–796.
- [6] W.-Y. Chang, A literature review of wind forecasting methods, *J. Power Energy Eng.* 2 (4) (2014).
- [7] B.C.L. de Figueirédo, G.R. Moreira, B. Stosic, T. Stosic, Multifractal analysis of hourly wind speed records in petrolina, northeast Brazil, *Revista Brasileira de Biometria* 32 (4) (2014) 599–608.
- [8] K. Falconer, *Fractal Geometry: Mathematical Foundations and Applications*, John Wiley & Sons, 2004.
- [9] J. Feder, *Fractals*, Springer Science & Business Media, 2013.
- [10] T. Feng, Z. Fu, X. Deng, J. Mao, A brief description to different multi-fractal behaviors of daily wind speed records over China, *Phys. Lett.* 373 (45) (2009) 4134–4141.
- [11] L. Fortuna, S. Nunnari, G. Guariso, Fractal order evidences in wind speed time series, in: *ICFDA'14 International Conference on Fractional Differentiation and its Applications 2014*, IEEE, 2014, pp. 1–6.
- [12] N.I. Fox, A tall tower study of Missouri winds, *Renew. Energy* 36 (1) (2011) 330–337.
- [13] J.W. Kantelhardt, S.A. Zschiegner, E. Koscielny-Bunde, S. Havlin, A. Bunde, H.E. Stanley, Multifractal detrended fluctuation analysis of nonstationary time series, *Phys. Stat. Mech. Appl.* 316 (1–4) (2002) 87–114.
- [14] R.G. Kavasseri, R. Nagarajan, A multifractal description of wind speed records, *Chaos, Solitons & Fractals* 24 (1) (2005) 165–173.
- [15] M. Laib, J. Golay, L. Telesca, M. Kanevski, Multifractal analysis of the time series of daily means of wind speed in complex regions, *Chaos, Solit. Fractals* 109 (2018) 118–127.
- [16] E. Li, X. Mu, G. Zhao, P. Gao, Multifractal detrended fluctuation analysis of streamflow in the yellow river basin, China, *Water* 7 (4) (2015) 1670–1686.
- [17] J. Ludescher, M.I. Bogachev, J.W. Kantelhardt, A.Y. Schumann, A. Bunde, On spurious and corrupted multifractality: the effects of additive noise, short-term memory and periodic trends, *Phys. Stat. Mech. Appl.* 390 (13) (2011) 2480–2490.
- [18] B. Mandelbrot, *The Fractal Geometry of Nature* Wh Freeman and Company new york, NY zbMATH, 1982.
- [19] B. Mandelbrot, *Fractals and Chaos: the Mandelbrot Set and beyond*, Springer Science & Business Media, 2013.
- [20] B.B. Mandelbrot, Self-affine fractals and fractal dimension, *Phys. Scripta* 32 (4) (1985) 257.
- [21] B.B. Mandelbrot, Fractal geometry: what is it, and what does it do? *Proceedings of the Royal Society of London. A. Mathematical and Physical Sciences* 423 (1864) 3–16, 1989.
- [22] M.S. Movahed, G. Jafari, F. Ghasemi, S. Rahvar, M.R.R. Tabar, Multifractal detrended fluctuation analysis of sunspot time series, *J. Stat. Mech. Theor. Exp.* (2) (2006) P02003, 2006.
- [23] D. Of Energy, Wind energy, 2019.
- [24] C.I. of Technology, *Atomic Fractals in Metallic Glasses*, 2015.
- [25] W.E.T. Office, Wind Energy in missouri, 2019.
- [26] P. Peebles, The fractal galaxy distribution, *Phys. Nonlinear Phenom.* 38 (1–3) (1989) 273–278.
- [27] K. Philippopoulos, N. Kalamaras, C.G. Tzanis, D. Deligiorgi, I. Koutsogiannis, Multifractal detrended fluctuation analysis of temperature reanalysis data over Greece, *Atmosphere* 10 (6) (2019) 336.
- [28] M.B. Ribeiro, A.Y. Miguelote, Fractals and the distribution of galaxies, *Braz. J. Phys.* 28 (2) (1998) 132–160.
- [29] H. Salat, R. Murcio, E. Arcuate, Multifractal methodology, *Phys. Stat. Mech. Appl.* 473 (2017) 467–487.
- [30] L. Salomao, J. Campanha, H. Gupta, Rescaled range analysis of pluviometric records in sao paulo state, Brazil, *Theor. Appl. Climatol.* 95 (1–2) (2009) 83–89.
- [31] P. Shang, Y. Lu, S. Kamae, Detecting long-range correlations of traffic time series with multifractal detrended fluctuation analysis, *Chaos, Solit. Fractals* 36 (1) (2008) 82–90.
- [32] D.L. Turcotte, *Fractals and Chaos in Geology and Geophysics*, Cambridge university press, 1997.
- [33] Y. Yuan, X.-t. Zhuang, X. Jin, Measuring multifractality of stock price fluctuation using multifractal detrended fluctuation analysis, *Phys. Stat. Mech. Appl.* 388 (11) (2009) 2189–2197.
- [34] X. Zhang, M. Zeng, Q. Meng, Multivariate multifractal detrended fluctuation analysis of 3d wind field signals, *Phys. Stat. Mech. Appl.* 490 (2018) 513–523.